Ceramics International 47 (2021) 22404–22415

Contents lists available at ScienceDirect

Ceramics International

journal homepage: www.elsevier.com/locate/ceramint

In-situ reaction synthesis Al_2O_3 overlay modified 7YSZ TBC for NaCl hot corrosion

Jia-Feng Fan [a,b,1], Guo Liu [c,1], Xue-Shi Zhuo [d,1], Xiao-Feng Zhang [b,c,e,*], Jun-Li Feng [f], Wo Jiang [g], Yan-Qing Jiang [g], Ju-Hang Yin [b], Bing He [b], Yong-Jun Hu [a], Rong-Jiu Li [a,b], Shuang-Quan Guo [h], Huan-Tao Chen [b], Chun-Ming Deng [b], Min Liu [b], Ke-Song Zhou [a,b,**]

[a] School of Materials and Energy, Guangdong University of Technology, Guangzhou, 510006, China
[b] National Engineering Laboratory for Modern Materials Surface Engineering Technology & The Key Lab of Guangdong for Modern Surface Engineering Technology, Institute of New Materials, Guangdong Academy of Sciences, Guangzhou, 510650, China
[c] Department of Mechanical Engineering City University of Hong Kong, Tat Chee Avenue Kowloon, Hong Kong, China
[d] State Key Laboratory for Manufacturing Systems Engineering, Xi'an Jiaotong University, Xi'an, 710049, China
[e] Foshan Taoyuan Institute of Advanced Manufacturing, Foshan, 528225, China
[f] Shenzhen Customs Industrial Products Inspection Technology Center, Shenzhen, 518067, China
[g] Praxair Surface Technologies, Wuxi, 213164, China
[h] Chengdu Holy(Group)Industry Co., Ltd., Chengdou, 610000, China

ARTICLE INFO

Keywords:
Marine environment
Plasma spray-physical vapor deposition
Al_2O_3-Modification
NaCl hot Corrosion

ABSTRACT

Thermal barrier coatings (TBCs) are facing the challenge of chloride salt hot corrosion in the marine environment. In the manuscript, 7YSZ feather-like columnar structure coatings were prepared by plasma spray-physical vapor deposition (PS-PVD). The Al_2O_3-modification based on in-situ synthesis was used as the strategy to improve the hot corrosion resistance of the coating. Then, the coatings were subjected to test of 900 °C NaCl thermal exposure and combustion gas-salt spray ablation. The microstructure and phase evolution results of the coatings show that NaCl has a strong corrosive effect on the as-sprayed PS-PVD TBC and leading to catastrophic oxidation. In contrast to this, the Al_2O_3-modified coating shows good corrosion resistance. In the hot corrosion behavior of NaCl, the metal elements in the bond layer are rapidly oxidized and accumulated on the surface of TGO layer through the electrochemical corrosion mechanism, which makes the TGO thicken rapidly. After combustion gas-salt spray corrosion, the YSZ coatings sintered and the evolution of mechanical properties were analyzed. Compared with the initial sprayed state, the hardness of the as-sprayed coating and the Al_2O_3-modified coating increased by 13.04 GPa and 11.47 GPa, respectively. And the elastic modulus of as-sprayed coating and Al_2O_3-modified coating increased by 133.00 GPa and 129.60 GPa, respectively.

1. Introduction

Thermal barrier coating (TBC) is an important thermal protection system in aviation turbine engine, which is used to deposit the surface of hot-section components to improve their upper limited temperature and thermal efficiency[1,2]. However, due to the high humidity and high salt environment, the thermal barrier coatings face the hot corrosion challenge when they service in carrier-based aircraft which frequently take off and land on the sea surface[3]. A typical TBC system consists of a 7YSZ (zirconia stabilized with 7 wt% yttrium) ceramic layer for thermal insulation and a MCrAlX (where M = Ni and Co, X = rare earth elements) metal layer for transition[4–6]. In the double-layer structure system, the difference of preparation technology of ceramic layer is one of the important factors affecting the performance of TBCs. The two main TBCs manufacturing routes of air plasma spraying (APS)[7,8] and electron beam-physical vapor deposition (EB-PVD)[9,10] to prepare ceramic layer with a typical splat microstructure (APS TBCs) and columnar microstructure (EB-PVD TBCs), respectively. However, owing

* Corresponding author. National Engineering Laboratory for Modern Materials Surface Engineering Technology & The Key Lab of Guangdong for Modern Surface Engineering Technology, Institute of New Materials, Guangdong Academy of Sciences, Guangzhou, 510650, China.
** Corresponding author. School of Materials and Energy, Guangdong University of Technology, Guangzhou, 510006, China.
E-mail addresses: zxf200808@126.com (X.-F. Zhang), kszhou2004@163.com (K.-S. Zhou).
[1] These authors contributed equally to this work.

https://doi.org/10.1016/j.ceramint.2021.04.250
Received 20 February 2021; Received in revised form 16 April 2021; Accepted 25 April 2021
Available online 12 May 2021

to the influence of the microstructures of the thermal barrier coatings prepared by the traditional technology, the thermal cycle life of the APS TBCs is short, and the thermal insulation performance of EB-PVD TBCs is low. Recently, an emerging preparation technology of plasma spray-physical vapor deposition (PS-PVD) has attracted much attention, and this technology has the ability to prepare feather-like columnar ceramic layer with high thermal cycle life and low thermal conductivity due to its low chamber pressure and fast vapor deposition characteristics [11–14]. The coating with feather-like columnar structure is expected to replace traditional thermal barrier coatings on aviation turbine engine.

Although the PS-PVD 7YSZ TBC good thermal insulation and high stress tolerance, this structure with open porosity also increases the risk of hot corrosion[15,16]. Premature failure event caused by hot corrosion in marine environment was observed for the first time in 1960s on the U.S. Navy shipboard[17,18]. Hot corrosion damage in the hot-section of the turbine hardware due to intrusion of salts (sulfates and chloride salts) from the marine air and/or from sulfur in the gas turbine combustion fuels was found to be the major reason behind the failure [19–21]. As the sources and hazards of hot corrosion are studied and reported, the impurity content in fuel is required to be controlled within a safe range as one of the measures to reduce the frequency of hot corrosion events. Nevertheless, the thermal barrier coatings still face the risk of hot corrosion from sea salt[22,23]. As the main component of sea salt, it is still not clear whether or not that NaCl has any significant role in hot corrosion. The hot corrosion effect of NaCl is questioned by some researchers, because the vapor pressure of chloride is so high that turbine possible is effectively exposed only to vapor-state NaCl, resulting in that NaCl or chloride per se is seldom found on corroded turbine components[24]. Another part of the research believes that NaCl mainly plays a secondary role in hot corrosion, and participates in hot corrosion as a substance that promotes the formation of Na_2SO_4[18]. Actually, the NaCl molten salt has been proved to be harmful to metal materials at high temperature. The corrosion mechanism can be divided into two types: one is to dissolve dense metal oxide scales by acid or alkaline dissolution mechanism, and then precipitate loose oxide scales to destroy the protective layer of the material; the other is electrochemical corrosion in molten salt, which is driven by the potential difference between anode and cathode to corrode metal material[25]. Therefore, the direct corrosion effect of NaCl on TBCs should not be ignored.

PS-PVD 7YSZ TBC needs to adopt an upgrade strategy to meet the challenges of hot corrosion. In order to prevent the corrosive molten salt to invade the coating, it is considered as an effective method to modify a physical barrier layer on the YSZ surface[26]. The physical barrier layer can roof the pores and cracks on the surface of 7YSZ, and can effectively prevent the infiltration of various molten salts. The material selection characteristics should have high temperature resistance, corrosion resistance and appropriate thermal expansion coefficient. Some studies have found that the laser and electron beam remelting modification method can produce a dense remelted layer with reticulated cracks on the surface of YSZ, which can block the infiltration of molten salt, but the remelted layer can reduce these performances of thermal insulation performance and thermal cycle life[27–29]. Other some studies found that Pd-Ag、Pd and Pt have good corrosion resistance and ability to prevent molten salt adhesion, but the cost of preparing barrier layer is high and high temperature stability needs to be solved[30]. Al_2O_3 is an ideal material as the physical barrier layer due to its good hot corrosion resistance and low cost[31]. However, the Al_2O_3 layer is usually sprayed directly on the surface of the YSZ thermal barrier coating, the bonding strength of the Al_2O_3 layer and the YSZ coating is poor, and the thermal cycle life needs to be improved[32]. Therefore, preparing an Al_2O_3 overlayer that can effectively block the infiltration of NaCl without significantly reducing the thermal cycle life and thermal insulation performance of the coating is the focus of research on the modification [33].

In this study, feather-like columnar structure 7YSZ thermal barrier coating was prepared by PS-PVD, and dense Al_2O_3 films were prepared on the surface of the coatings by in-situ synthesis. After this, thermal exposure of NaCl and combustion gas-salt spray hot corrosion was carried out to study the NaCl hot corrosion behavior and corrosion mechanism of the coating. The Al_2O_3-modification process for 7YSZ TBCs prepared by PS-PVD was expected to weaken the marine hot corrosion attack.

2. Experimental procedures

2.1. Sample preparation

During the experiment, the bond layer and ceramic layer were prepared through the PS-PVD multicoat system (Oerlikon Metco). Agglomerated 7YSZ powder, designated as M6700 (Oerlikon Metco) and NiCrAlY metal powder (Amdry 413, Oerlikon Metco) were used as the feedstock materials. Disks made of superalloy DZ40 M with a diameter of 25.4 mm were used as the substrates having rounded topside edge, which is used for NaCl thermal exposure. The combustion gas-salt spray hot corrosion sample substrates are 7 mm diameter superalloy rod due to clamping requirements. The TBCs were obtained by successive deposition of 150 μm thick NiCrAlY bond layer and 200 μm YSZ coating on the substrate via PS-PVD. As for Al_2O_3-modification, firstly obtained the Al-deposited 7YSZ coatings by magnetron sputtering (J-1250, Jingzhou Industrial Coating, China). The thickness of the Al film is controlled by the deposition time, and deposited on the surface of the corresponding samples for 3, 4, 5, 6, 7, 8 and 9 h respectively. Finally, vacuum heat treatment in the temperature range of 606 °C–980 °C was carried out on the Al-deposited TBCs samples, and thereby forming the Al_2O_3-modified 7YSZ TBCs.

2.2. Water quenching and hot-corrosion test

The thermal cycling of the coatings was tested by holding at 1100 °C for 10 min in the furnace and quenching to room temperature as a cycle. And the deionized water at room temperature is used as quenching water. The evolution process of the coatings was recorded. Hot corrosion studies of the samples were carried out by thermal exposure of NaCl and combustion gas-salt spray at 900 °C in the presence of air, as show in Fig. 1. In the thermal exposure, the 20 mg/cm^2 sodium chloride was coated on the surface of the samples to be tested and kept in 900 °C furnace for 100 h. A burner (RFY-2) was used for the studies of combustion gas-salt spray hot corrosion according to the standard HB 7740-2004, holding the sample for 24 h followed by air cooling to room temperature as a cycle. Sodium chloride solution having concentration of 20 ppm was sprayed at a rate of 0.2 L/h as the source of salt and aviation commercial kerosene was controlled at 0.2 L/h during the testing.

2.3. TBCs characterization

Microstructures of the specimens were characterized by field emission-scanning electron microscope (FE-SEM, Nova-Nono430, FEI) and transmission electron microscope (TEM, JEOL-2100F) assisted with focused ion beam (FIB, 450S, FEI) milling. And phase transformation was characterized by X-ray diffraction (XRD, D8-Advance, Bruker) with a step of 0.02° (Cu-Kα, incident angle 3°, a 2θ range of 10-90°). The mechanical properties of the 7YSZ ceramic layer were evaluated by nano-indentation technique at a load of 30 mN using the nano-indenter (Anton Paar) with a Berkovich (tip radius <150 nm). The load-displacement curve during the loading-unloading cycle is obtained by nano-indentation test, as shown in Fig. 2. The hardness can be calculated by formula (13), [34]:

$$H = \frac{P}{A} \tag{1}$$

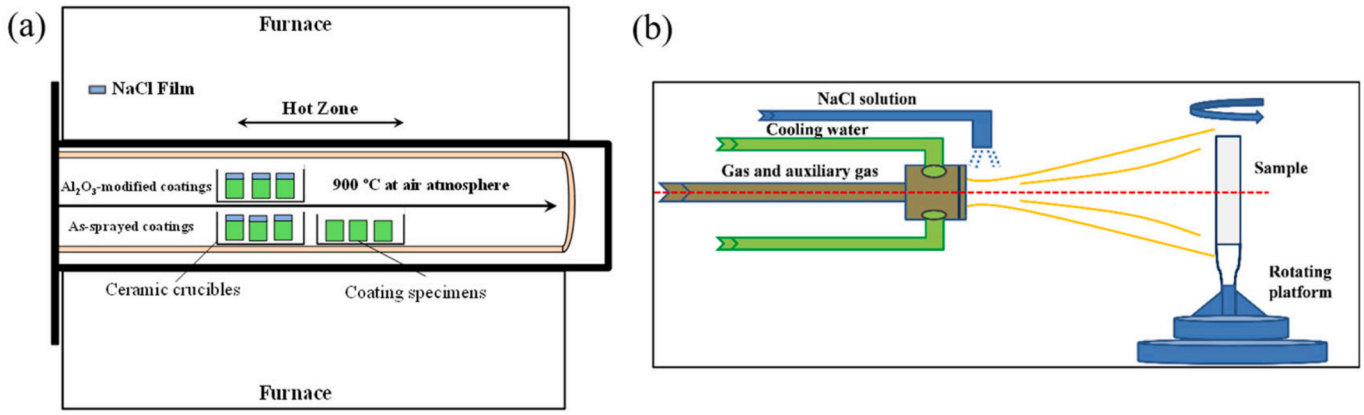

Fig. 1. Schematic diagram of hot corrosion test, (a) NaCl thermal exposure, (b) combustion gas-salt spray.

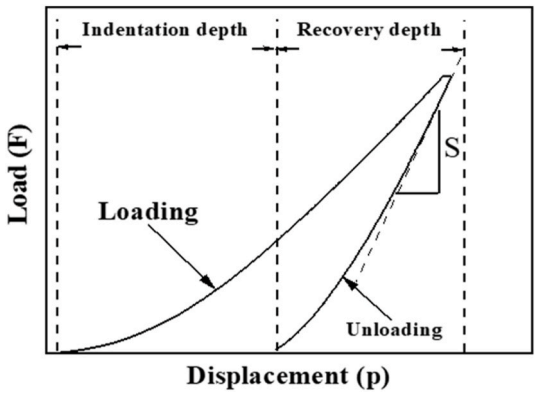

Fig. 2. Schematic diagram of nano-indentation load-displacement curve.

where, P is the indentation load and A is the projection area of the contact between the indenter and the sample.

Elastic modulus (E) can be calculated by formula (14):

$$E_r = \frac{\sqrt{\pi}\cdot S}{2\beta\cdot\sqrt{A}}$$

$$\frac{1}{E_r} = \frac{1-v^2}{E} - \frac{1-v_i^2}{E_i} \tag{2}$$

where, E_r is the elastic modulus of the tested system, E_i is the elastic modulus of the test indenter, β is a constant, β = 1.034, S is the contact stiffness and the value is the slope of the no-load linear section, υ = 0.04 is the Poisson's ratio of the tested material, and $\upsilon_i = 0.07$ is the Poisson's ratio of the diamond indenter.

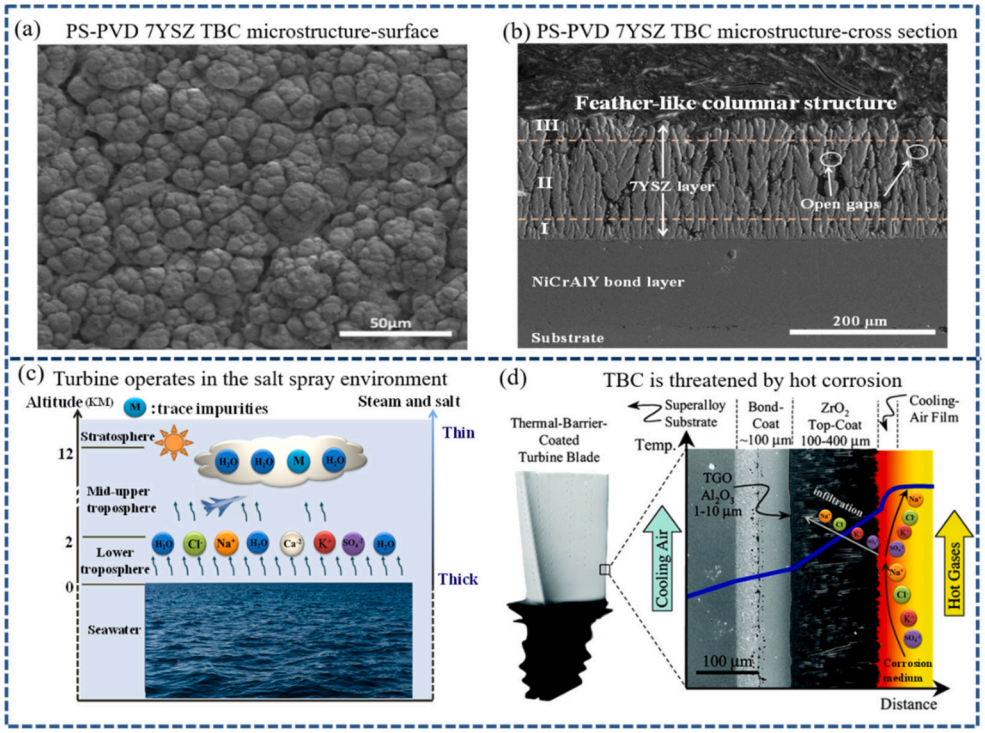

Fig. 3. PS-PVD 7YSZ TBC microstructure and marine hot corrosion, (a) PS-PVD coating surface, (b) PS-PVD coating cross-section, (c) schematic diagram of salt spray distribution on the sea surface, (d) thermal barrier coating molten salt hot corrosion.

3. Results and discussion

3.1. Coating design and preparation

Fig. 3 shows the microstructure of 7YSZ thermal barrier coating prepared by PS-PVD and marine hot corrosion factors. It can be seen that the coating surface presents "cauliflower head" shape, which is the top structure of columnar crystals clustered together. As shown in Fig. 3(b), the 7YSZ ceramic layer has loosened feather-like columnar structure in the cross-section, where are many longitudinal gaps almost penetrating the YSZ layer between the columnar crystals. The feather-like columnar structure of the coating can be divided into a dense area I at the bottom, a columnar crystal area II in the middle, and a bifurcation area III at the top. Among them, the columnar crystal area II has a large gap, and under the dense area I is a metal layer with a dense layered structure. The loose feather-like columnar structure of PS-PVD 7YSZ thermal barrier coating has good thermal insulation performance and thermal cycling performance. However, due to the open gaps in the ceramic layer can become a channel for molten salt to invade rapidly, the thermal barrier coating to face the risk of hot corrosion in the marine environment with high corrosive media[14].

In order to enhance the corrosion resistance of PS-PVD 7YSZ TBC, a dense layer was designed to cover the coating surface. Firstly, Al films were deposited on the surface of 7YSZ coating by magnetron sputtering, and in-situ reaction (Eq. (1)) was carried out during vacuum heat treatment, as shown in the Al_2O_3-modification schematic diagram (Fig. 4(a)). Then, according to the different Al-deposition time, the samples of 2, 3, 4, 6, 7 and 8 h were prepared to obtain Al_2O_3-modified TBCs. Fig. 4(b–f) shows the evolution process of the surface morphology of the samples in thermal shock. Before the thermal shock of the Al_2O_3-modified samples, the residual Al content on the surface increased with the increase of the Al-deposition time, resulting in a gradual blackening of the surface of the 2–8 h samples. With the implementation of thermal shock, the residual Al on the surface of the Al_2O_3-modified samples was completely oxidized, and the color of the coatings surface turned white. After the 28 cycles thermal shock, the coatings began to peel off gradually. In the thermal shock performance test results of the sample, the 6 h Al_2O_3-modified coating has a good thermal shock performance close to that of the as-sprayed coating, and has a thicker modified overlay due to longer Al-deposition time. Therefore, in order to improve the surface compactness of the coating to resist hot corrosion, the 6 h Al_2O_3-modified sample was considered to be used for the improved coating.

$$3Al + 3ZrO_2 = 2Al_2O_3 + 3Al_3Zr \quad (3)$$

As shown in Fig. 5, it is the microstructure of the 6 h Al_2O_3-modified coating. There is a continuous overlayer on the surface of the coating, which fills the gap of the "cauliflower" structure, and the Al_2O_3-modification does no impact the internal structure of the coating. Subsequently, the EDS and XRD patterns confirmed that the overlayer is mainly composed of dense and corrosion-resistant α-Al_2O_3.

3.2. Microstructural evolution of Al_2O_3-modified PS-PVD 7YSZ TBCs under NaCl thermal exposure

The NaCl hot corrosion performance of PS-PVD 7YSZ TBC was studied by NaCl thermal exposure experiment. Fig. 6 shows the macroscopic morphology of PS-PVD 7YSZ thermal barrier coating after NaCl thermal exposure for 100 h. The as-sprayed coating is basically maintained complete morphology which thermal exposure in air, and the color of the coating turns yellow owing to the oxygen content in the YSZ lattice is increased after corrosion. However, another as-sprayed coating has a degeneration under the NaCl attack, and the substrate at

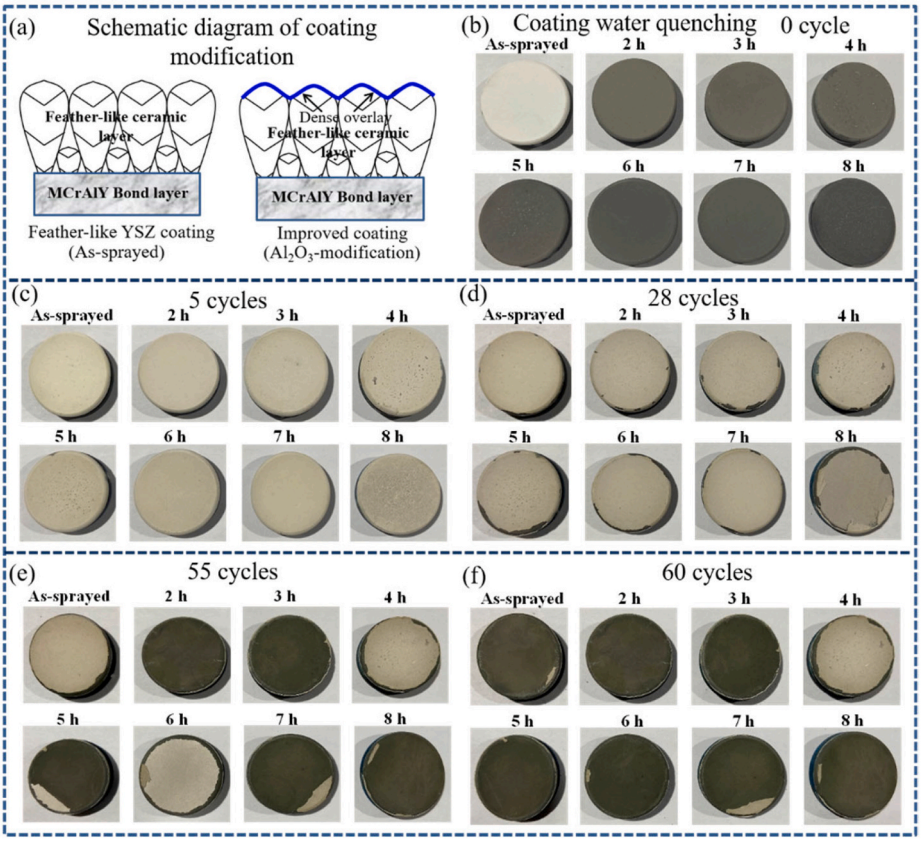

Fig. 4. The modification schematic diagram and thermal shock properties of coatings with different Al-deposition times. (a) PS-PVD 7YSZ TBCs Al2O3-modification diagram. (b) Images of as-sprayed coating and Al-modified coatings before water quenching. (c) 5 cycles of water quenching. (d) 28 cycles of water quenching. (e) 55 cycles of water quenching. (f) 60 cycles of water quenching.

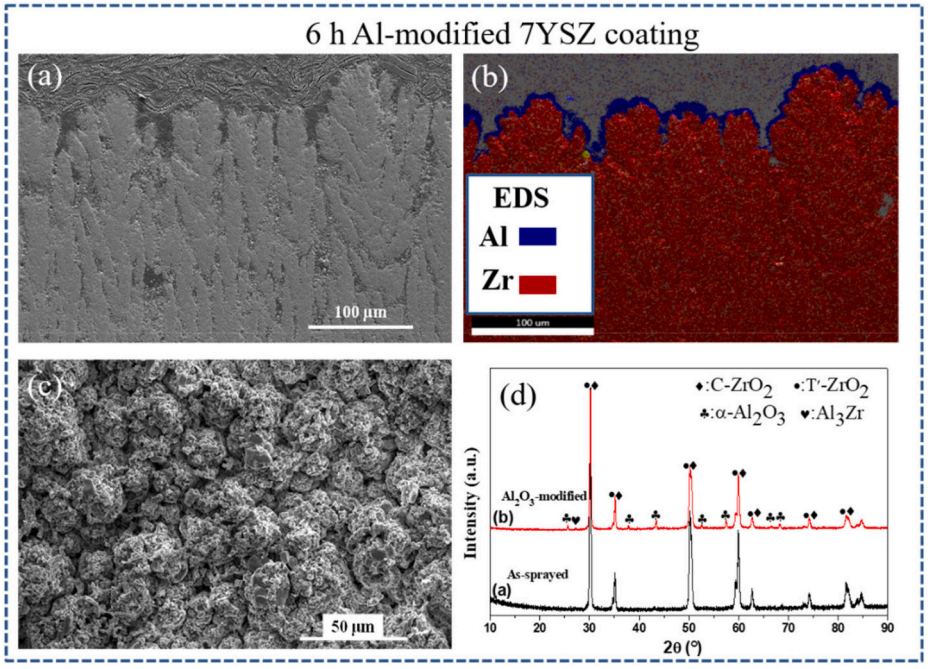

Fig. 5. Microstructure of 6 h Al-modified coating, (a) cross-section morphology, (b) element distribution. (c) Surface morphology, (d) phase evolution after modification.

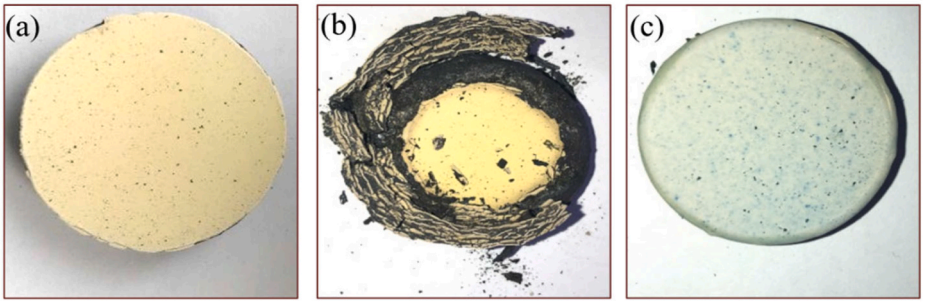

Fig. 6. Macroscopic morphology of PS-PVD 7YSZ thermal barrier coating after NaCl thermal exposure for 100 h, (a) as-sprayed coating thermal exposure in air, (b) as-sprayed coating thermal exposure with NaCl, (c) Al_2O_3-modified coating thermal exposure with NaCl.

the edge is seriously damaged, resulting in severe wrinkling and delamination of the coating. It is revealed that as-sprayed PS-PVD 7YSZ TBCs are suffered hot corrosion by NaCl. In contrast, the surface of the Al_2O_3-modified coating under NaCl attack without significant degradation. It is worth noting that after the PS-PVD 7YSZ TBC was subjected to NaCl hot corrosion, no new phases were found in the XRD pattern of the corresponding ceramic layer, as shown in Fig. 7, which indicates that NaCl has no significant thermochemical effect on the 7YSZ ceramic layer. Fig. 8 shows the evolution of the microstructure of the PS-PVD 7YSZ thermal barrier coating under the action of NaCl hot corrosion and Al_2O_3- modification during thermal exposure. The surface of as-sprayed coating still maintains "cauliflower" morphology under the thermal exposure in air. But after NaCl thermal exposure, the cauliflower-like grains on the as-sprayed coating surface appear sintered, and the surface structure becomes dense, as can see in Fig. 8(b1). As for the Al_2O_3-modified coating, the "cauliflower" grains on the coating are still wrapped by glazed overlay after NaCl thermal exposure, showing a compact surface morphology. The cross-section microstructure of the coatings after thermal exposure are given in Fig. 8(a2-a3, b2-b3, c2-c3). In the absence of NaCl, as-sprayed coating shows typical high-temperature oxidation phenomenon with thickening of the thermal growth oxide layer (TGO) and interlayer oxidation in the bond layer. It is

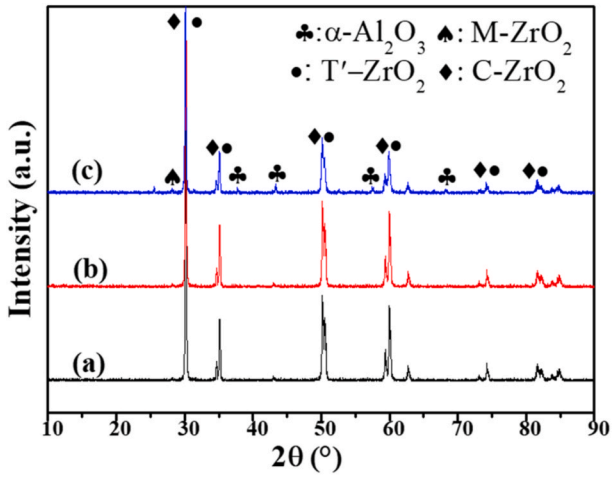

Fig. 7. XRD pattern of PS-PVD 7YSZ thermal barrier coating after thermal exposure, (a) as-sprayed coating thermal exposure in air, (b) as-sprayed coating thermal exposure with NaCl, (c) Al_2O_3-modified coating thermal exposure with NaCl.

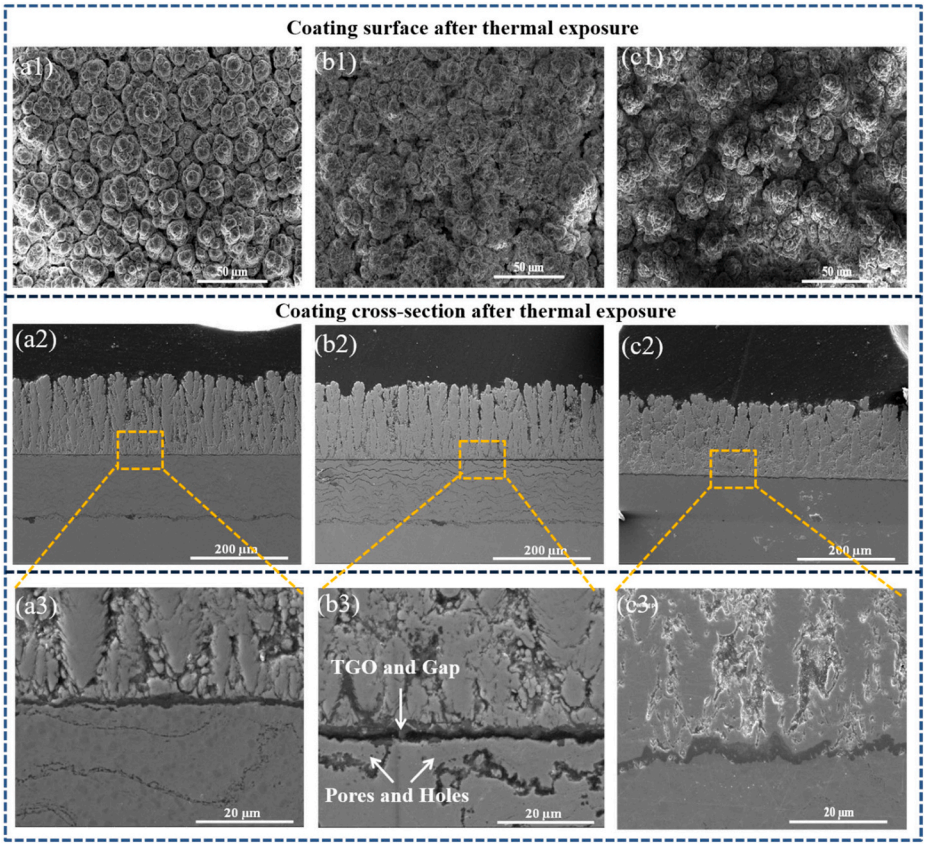

Fig. 8. Microstructure of PS-PVD 7YSZ thermal barrier coating after thermal exposure, (a1), (a2) and (a3) as-sprayed coating thermal exposure in air, (b1), (b2) and (b3) as-sprayed coating thermal exposure with NaCl, (c1), (c1) and (a3) Al_2O_3-modified coating thermal exposure with NaCl.

worth noting that in comparison to the other positions, the TGO layer is thicker under the columnar crystal gap. This is because the open gap becomes a fast channel for oxygen diffusion, which increases the tendency of metal oxidation. Fig. 8(b2) and 8(b3) show that the as-sprayed coating suffered catastrophic oxidation under NaCl attacked, resulting in the delamination of 7YSZ layer and metal layer at the TGO, and thick oxidation stripes and a large number of voids were densely distributed in the metal bond layer. In addition, TGO even intrudes in the columnar crystal gap at the bottom of 7YSZ layer due to the TGO rapid growth caused by severe oxidation. On the contrary, the bond layer of the Al_2O_3-modified coating is well protected under NaCl attack, and there is no obvious interlayer oxidation, and only a thick and continuous integrity TGO is displayed at the interface between YSZ and the bond layer. In summary, the NaCl thermal exposure experiment results show that the 7YSZ ceramic layer has good high temperature stability under NaCl hot corrosion, but the NaCl causes catastrophic oxidation of metal layer, significantly thickens TGO, and makes thermal barrier coating crack and delamination at TGO interface under the effect of thermal growth stress. In addition, the microstructure of Al_2O_3-modified PS-PVD 7YSZ TBC shows slight degradation, which indicates that the Al_2O_3-modification process can improve the NaCl hot corrosion resistance of the feather-like columnar structure coating.

3.3. Microstructural evolution of Al_2O_3-modified PS-PVD 7YSZ TBCs under combustion gas-salt spray hot corrosion

In fact, NaCl in the marine environment is usually in the form of salt spray when it is inhaled into aero-engines, which acts on the thermal barrier coating and is accompanied by the ablation of combustion gas. Therefore, in order to further evaluate the NaCl hot corrosion behavior for thermal barrier coating in the marine environment, the combustion gas-salt spray test was carried out. Fig. 9 shows the surface morphology of the coatings after 50 cycles combustion gas-salt spray hot corrosion. The as-sprayed coating basically maintains the original "cauliflower" characteristics, but due to the gas ablation, the "cauliflower" gains become loose and porous. In addition, due to insufficient combustion of the gas, some adsorptive carbon particles remained on the surface of the coating. The elemental composition analysis of the carbon particles revealed the presence of trace amounts of S and Cl corrosive elements were present in the ablation process. After a long period of combustion gas-salt spray ablation of Al_2O_3-modified coating, the microstructure change on the surface is still not obvious. The XRD patterns revealed the phase evolution of the coating after 50 cycles of hot corrosion, as can see in Fig. 10. Similar to the thermal exposure effect of NaCl, the corresponding XRD patterns of the coatings before and after the combustion gas-salt spray ablation basically remain unchanged. But it's worth noting that a smaller m-ZrO_2 peak of appears on the as-sprayed coating after corrosion, which indicate that some tetragonal or cubic zirconia in the YSZ layer transforms into monoclinic phase. It is speculated that due to the corrosive elements such as vanadium in the fuel, the vanadate produced after combustion will react and consume the Y_2O_3 in YSZ, resulting in the unstable phase transformation of zirconia. This similar phenomenon is commonly reported by YSZ in hot corrosion containing vanadate[18].

The cross-sectional microstructures of the coatings after 50 cycles of combustion gas-salt spray hot corrosion are given in Fig. 11. The as-sprayed coatings show significant degradation, but different from thermal exposure of NaCl, the YSZ layer shows serious sintering phenomenon, the columnar crystal gap decreases and the average size of secondary grains on the columnar crystal grows to 365 Å. In addition, the bond layer presents finer interlayer oxidation. Correspondingly, the Al_2O_3-modified PS-PVD 7YSZ coating has better performance during the

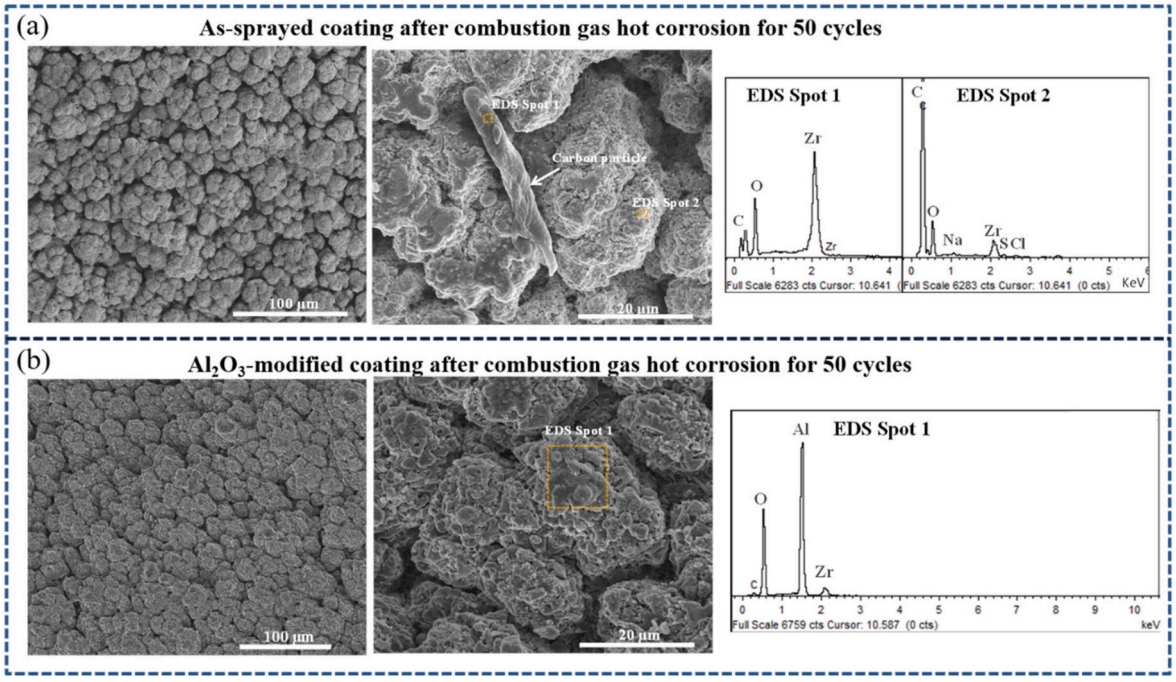

Fig. 9. Surface morphology of PS-PVD 7YSZ TBC after combustion gas-salt spray hot corrosion, (a) as-sprayed coating, (b) Al_2O_3-modified coating.

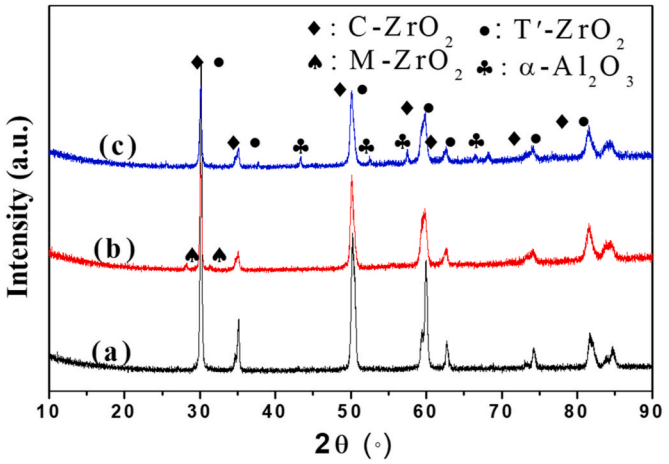

Fig. 10. XRD patterns of PS-PVD 7YSZ TBC before and after combustion gas-salt spray hot corrosion, (a) as-sprayed coating before corrosion, (b) as-sprayed coating after corrosion, (c) Al_2O_3-modified coating after corrosion.

corrosion test with less damage, as can see in Fig. 11(b). The average grain size of the secondary grain in the YSZ layer was only grow to 242 Å, and the bond layer showed a slighter oxidation.

In order to further reveal the influence of the combustion gas-salt spray on the 7YSZ coating, the mechanical properties of the ceramic layer after corrosion were evaluated by nano-indentation. The nano-indentation displacement load curve (Pd-Fn curve) of PS-PVD 7YSZ coatings columnar crystal region (II region) is given in Fig. 12. It can be observed from the Pd-Fn curves of the initial as-sprayed coating that the average recovery depth of indentation is 132.0 nm and the average indentation depth is 228.0 nm after unloading. As for the after 50 cycles combustion gas-salt spray hot corrosion, the toughness of the coatings is significantly decreased. The average recovery depth and indentation depth of the as-sprayed coating is 117.8 nm and 163.2 nm, respectively. Correspondingly, the average recovery depth and indentation depth of the Al_2O_3-modified coating is 123.5 nm and 175.0 nm, respectively. Fig. 13 shows the evolution of mechanical properties of the coatings in columnar crystal region after hot corrosion. After hot corrosion, the mechanical properties of the coatings are degeneration, and the harness and elastic modulus of the coatings are significantly higher than those of the initial as-sprayed coating. It is worth noting that the hardness and elastic modulus of the Al_2O_3-modified coating (H = 19.38 GPa, E = 219.2 GPa) are still lower than that of the as-sprayed coating (H = 20.95 GPa, E = 222.6 GPa). It indicates that the Al_2O_3-modification process is beneficial to improve the corrosion resistance of PS-PVD 7YSZ coating and slow down the deterioration of mechanical properties of the coating. The reason may be that the Al_2O_3 overlayer acts as a dense barrier layer, which insulates the impact of corrosive medium and combustion gas directly on the interior of the coating and reduces the sintering degree of the coating. In fact, the coating with the excellent mechanical properties generally have a high stress tolerance, which improves the thermal cycle life of the coating to a certain extent. Al_2O_3-modification process slows down the deterioration of mechanical properties and reduces the risk of TBCs spalling caused by mechanical properties deterioration. This avoids the premature direct exposure of the superalloy blades to the outside, which is of great significance to the marine environment with high salt content.

3.4. NaCl hot corrosion behavior and mechanism

Presently available literature reports on the marine hot corrosion, the effect of NaCl is often considered not important in hot corrosion due to the vapor pressure of chloride is very high at high-temperature so that it is difficult to find corrosion products containing chlorine after corrosion events[35]. However, in the present study shows strong hazards of NaCl at high temperature, leading to serious oxidation of the coating under thermal exposure. In order to reveal the corrosion mechanism of NaCl, the oxide phase in the as-sprayed coating generated under the thermal exposed of NaCl was analyzed, and can be seen in Fig. 14. Fig. 14(a1) shows that the residual TGO structure at the bottom of 7YSZ is still uniform and dense, and then the TGO slice at the YSZ gap is obtained by focused ion beam (FIB). Elemental analysis of the FIB slice showed that composition of the TGO grown in the gap of ceramic layer was still mainly composed of Al_2O_3. The subsequent diffraction pattern

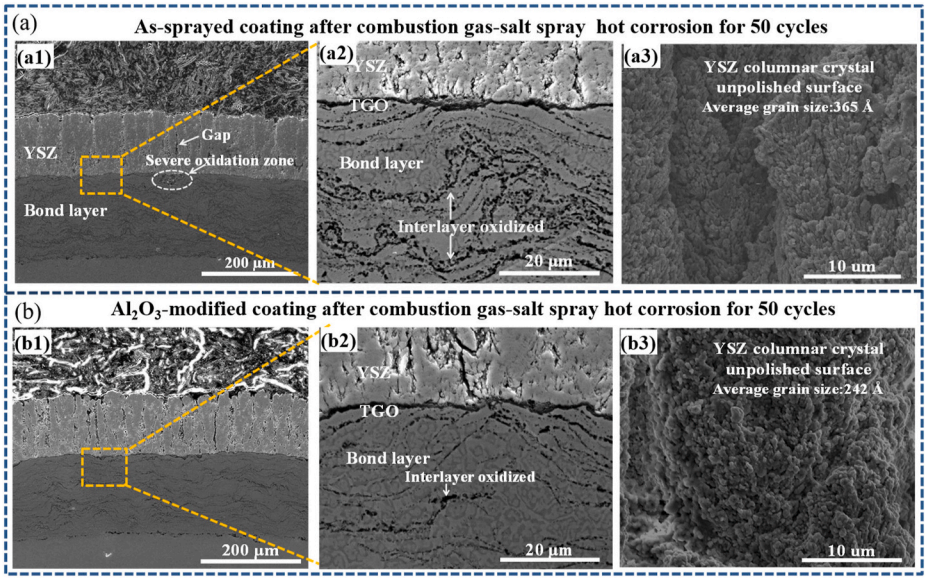

Fig. 11. Surface morphology of PS-PVD 7YSZ thermal barrier coating after combustion gas-salt spray hot corrosion, (a1-3) as-sprayed coating (b1-3) Al_2O_3-modified coating.

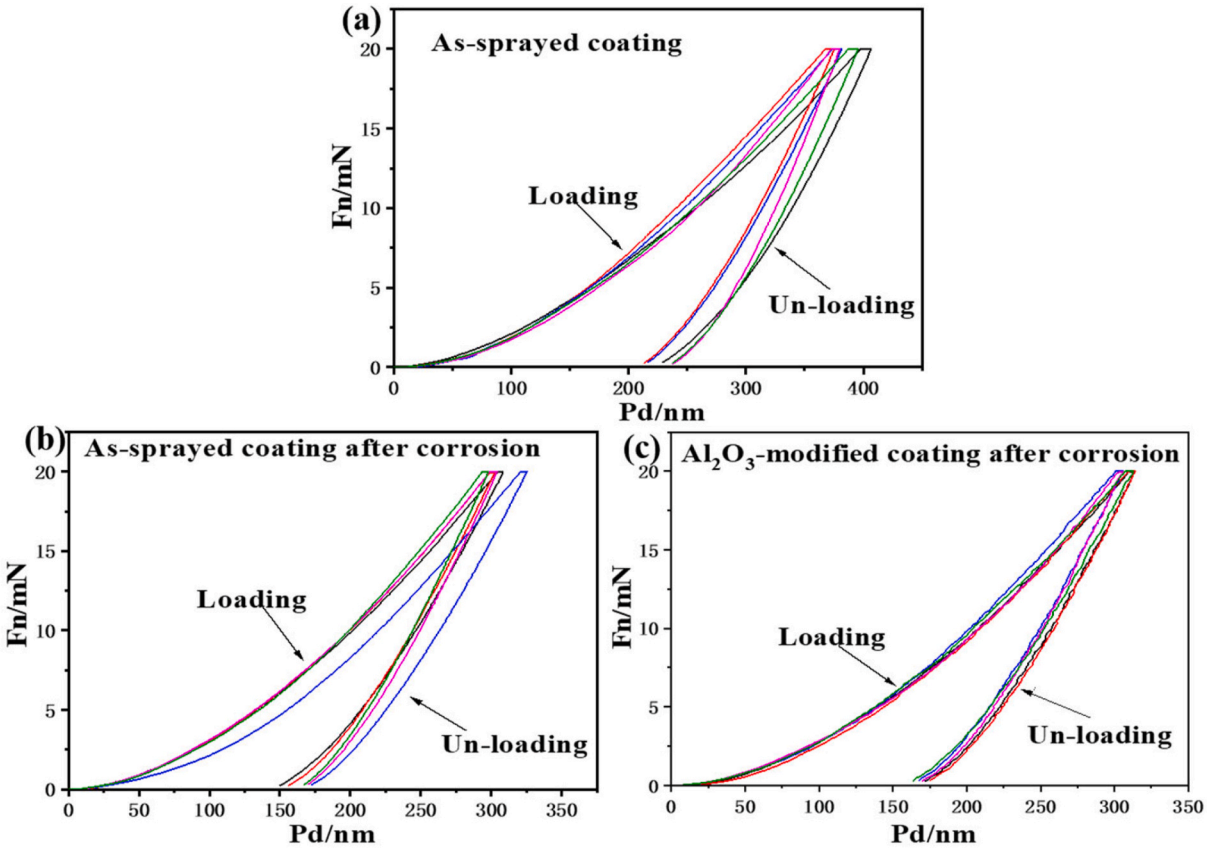

Fig. 12. The nanoindentation displacement load curve of PS-PVD 7YSZ coatings columnar crystal region (II area). (a) Initial as-sprayed coating feather-like columnar crystal Pd-Fn curves. (b) As-sprayed coating Pd-Fn curves after combustion gas-salt spray hot corrosion. (c) Al_2O_3-modified coating Pd-Fn curves after combustion gas-salt spray hot corrosion.

confirmed that the TGO in the section position was α-Al_2O_3. Fig. 14(b1) reveals the microstructure of the oxidation in the bond layer which shows the presence of a large number of pores. Moreover, the FIB was used to cut the interlayer oxides in the bond layer, and it was found out that though the interlayer oxides at the slice were also mostly alumina, further TEM analysis showed that the oxides were specifically β-Al_2O_3.

In the current research on the mechanism of sea salt thermal corrosion, Goebel and Pettit et al. early established early a salt solubility mechanism model based on Na_2SO_4 for explain the alloy catastrophic oxidation under the protection of the oxide scales[36–38]. This model

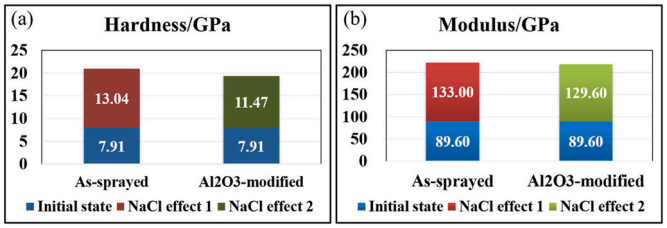

Fig. 13. Evolution of mechanical properties of PS-PVD 7YSZ coatings in columnar crystal region (II region), (a) hardness before and after hot corrosion, (b) elastic modulus before and after hot corrosion.

deems that there is a thermodynamic equilibrium in molten Na_2SO_4 (Eqn. (4) and Eqn. (5)):

$$Na_2SO_4 = Na_2O + SO_3 \tag{4}$$

$$SO_3 = \frac{1}{2}S_2 + \frac{3}{2}O_2 \tag{5}$$

Among them, Na_2O is regarded as the alkaline component of molten salt, SO_3 is the acidic component, lga_{Na_2O} and lgP_{SO_3} are defined as the alkalinity and acidity of molten salt, respectively. The oxidation of metal or alloy under the molten salt film will consume oxygen, which will promote Eqn. (5) equation forward, resulting in the decrease of P_{SO_3} at the oxide/molten salt interface. According to Eqn. (4), that is equivalent to the increase of a_{Na_2O}, resulting in the alkaline dissolution of Al_2O_3 (Eqn. (6)):

$$Al_2O_3 + O^{2-} = 2AlO_2^- \tag{6}$$

Since the alkalinity of the molten salt layer decreases from the inside to the outside, the AlO_2^- diffuses outward in the salt layer, it will decompose and deposit loose and unprotected Al_2O_3 in the molten salt.

$$2AlO_2^- = Al_2O_3 + O^{2-} \tag{7}$$

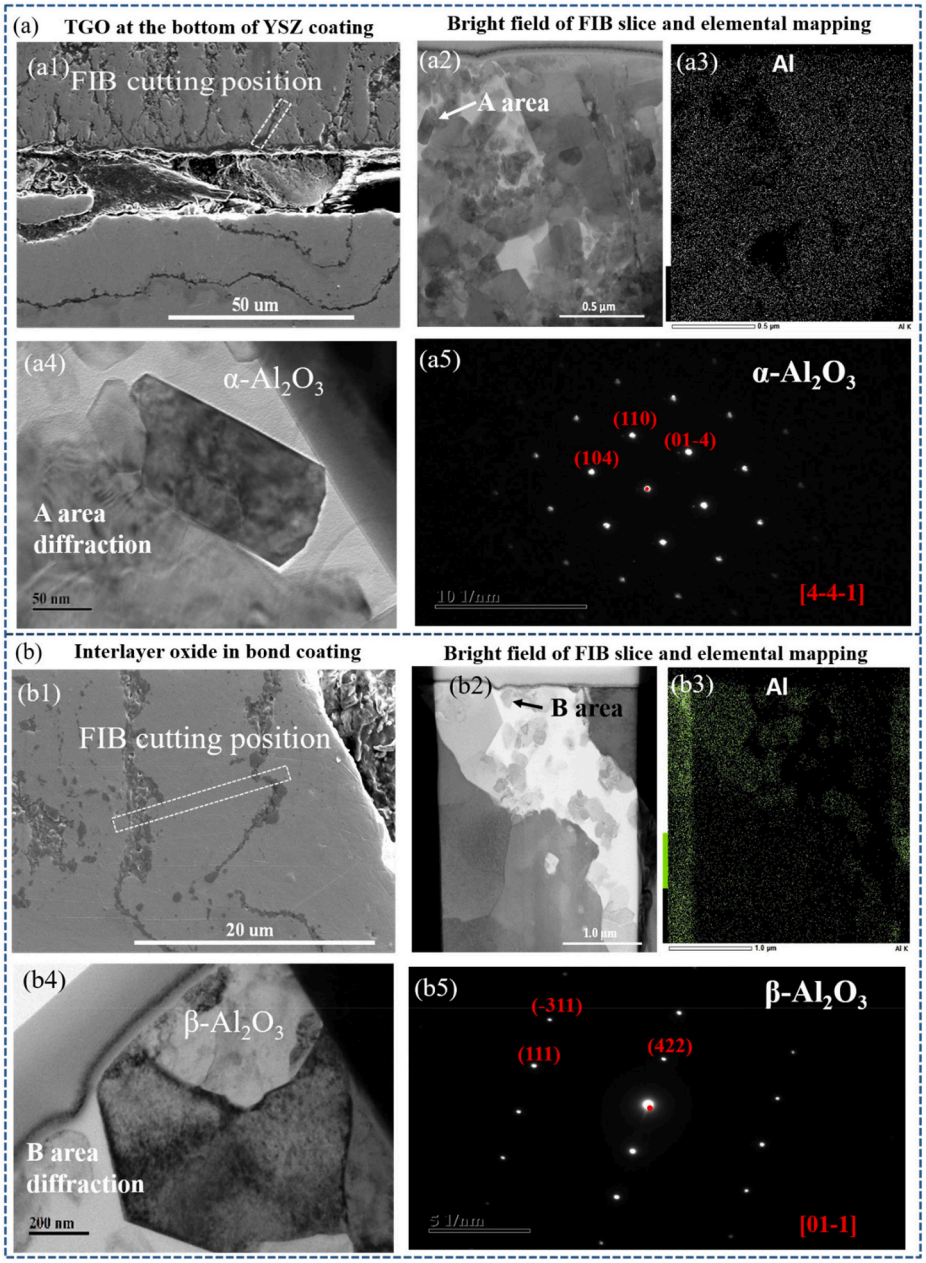

Fig. 14. Phase analysis of the oxide in the as-sprayed TBC under NaCl attack, (a1) FIB cutting region in TGO, (a2) TGO FIB slice bright field imaging, (a3) Al element distribution in FIB slice, (a4) enlarged view of bright field in area A, (a5) electron diffraction pattern of A aera grain, (b1) FIB cutting region in bond layer, (b2) interlayer oxide FIB slice bright field imaging, (b3) Al element distribution in FIB slice, (b4) enlarged view of bright field in area B, (b5) electron diffraction pattern of B aera grain.

The hot corrosion behavior of this model is summarized as the alkaline or acidic dissolution of protective metal oxides at the oxide/molten salt interface, while the process of depositing and forming loose oxides at the molten salt/gas-phase interface.

According to the evolution of the coating structure after corrosion, the Na_2SO_4 hot corrosion model is not suitable to explain the corrosion behavior of NaCl. If NaCl attacks TGO through salt dissolving corrosion behavior in the coating, and then the metal bond layer is severely oxidized. According to the corrosion kinetics, a loose oxide layer should be formed the interface between YSZ and metal layer after thermal exposure. However, as shown in Figs. 8 and 14, TGO still maintains the densified α-Al_2O_3 crystal form after NaCl corrosion, which indicates that NaCl does not melt and re-deposit Al_2O_3 through alkaline or acidic dissolution. In fact, molten salt is deposited on the surface of the oxide film, even if it does not dissolve with the oxide, but as an excellent ionic conductor, it has an important influence on the ionic behavior in the oxidation reaction, so the corrosion behavior of NaCl should be considered as the electrochemical corrosion model[35]. In the metal bond layer, Al due to its low electronegativity that will be priority to react as anode (Eqn. (8)):

$$Al = Al^{3+} + 3e \tag{8}$$

Assuming that at the TGO/7YSZ interface, only oxygen that penetrates into the 7YSZ layer participates in the cathode reduction reaction (Eqn. (9)):

$$\frac{1}{2}O_2 + 2e = O^{2-} \tag{9}$$

This total reaction formula is

$$Al + \frac{1}{2}O_2 = Al_2O_3 \tag{10}$$

Although Al element has low electronegativity and is easily oxidized, it is well known that under the protection of dense oxide film, the reaction rate of formula 9 is restricted by the diffusion rate of Al^{3+} and O^{2-} in dense Al_2O_3. In the result of the thermal exposure of the coating shown in Fig. 8(a1-a3), the as-sprayed coating is only corroded by oxygen alone, and it is difficult to achieve catastrophic oxidation even at a high temperature of 900 °C. Therefore, NaCl plays a key role in the catastrophic oxidation of the coating.

In the initial stage of NaCl hot corrosion, there is sufficient Cl^-, the adequate of Cl^- should be considered for the cathodic reduction reaction:

$$O_2 + Cl^- + 3e = 2O^{2-} + \frac{1}{2}Cl_2 \tag{11}$$

Therefore, the reaction (10) should be revised as:

$$Al + O_2 + \mathrm{NaCl} = \mathrm{NaAlO_2} + \frac{1}{2}Cl_2(g)\ \Delta G^{\theta} = -598.20 kj{\cdot}mol^{-1}\ at\ 900^{\circ}C \tag{12}$$

In Eqn. (12), Al reacts at the anode to form Al^{3+} ions, which migrate to the TGO/YSZ interface through diffusion, and react with oxygen and Cl^- to form AlO^{2-} ions. AlO^{2-} leaves the TGO interface and continuing to migrate in the YSZ direction, it will decompose to form Al_2O_3 as the O^{2-} concentration decreases (Eqn. (13)).

$$2AlO_2^- = Al_2O_3(s) + O^{2-} \tag{13}$$

In summary, the corrosion behavior of NaCl is not suitable to be explained by the dissolved salt deposition model, but conforms to the electrochemical corrosion model. The metal on one side of TGO quickly loses electrons and turns into ions, and then migrates to the other side of TGO in the form of ions, and reacts with oxygen to form metal oxide. In this process, the key intermediate reaction Eqn. (12) involved in NaCl reduces the oxygen content by one-third compared to the direct formation of oxides.

In the as-sprayed coating, owing to the continuous oxidation and ion migration of the metal bond layer, atomic vacancies are formed in the interlayer oxidation, resulting in a large number of holes and voids. However, due to the catastrophic corrosion at the edge, the as-sprayed coating lost the complete morphology of TGO formed by ion migration. In order to further demonstrate the viewpoint of electrochemical corrosion model, as shown in Fig. 15, it is the microstructure of TGO after corrosion of Al-modified coating. The upper and lower regions of TGO after NaCl corrosion show different contrast in the backscatter mode. The corresponding EDS analysis shows that the main element of TGO is Al, but Cr is mixed in the dark lower region, and Ni is mixed in the gray upper region. This delamination phenomenon is caused by the migration rate of different metal ions during the electrochemical corrosion process. In the process of TGO growth, the growth direction is from the bottom to the top. But the Ni electronegativity and ion radius are larger than the other two elements, the oxidation of Ni is slower, resulting in the lowest Ni ion concentration gradient and diffusion rate. Therefore, the deposition region of Ni is relatively backward. In addition, the morphology of the metal bond layer of the Al modified coating in the backscatter mode proves that oxygen does not directly and significantly erode the metal at this position, indicating that TGO is still continuous and dense during the corrosion process.

In the process of combustion gas-salt spray corrosion, because the fuel contains trace s element, NaCl is unstable in this oxidation environment [39], and the reaction equation Eqn. (14) will occur to form Na_2SO_4.

$$2NaCl + SO_3 + \frac{1}{2}O_2 = Na_2SO_4 + Cl_2 \tag{14}$$

In addition, due to the large amount of water in the salt spray, the reaction will also occur:

$$2NaCl + SO_3 + H_2O = Na_2SO_4 + 2HCl \tag{15}$$

Na_2SO_4 and HCl have harmful damage to the oxide film at 900 °C that will result in alkaline or acidic dissolution of the dense protective film. Therefore, the combustion gas-salt spray corrosion did not cause the 7YSZ coating to generate too thick TGO, on the contrary, the TGO structure under the columnar crystal gap of 7YSZ became loose, as shown in Fig. 11. Without the protection of TGO, the metal layer formed fine interlayer oxidation under the action of sufficient oxygen.

4. Conclusions

The 7YSZ TBCs with feather-like columnar microstructure were prepared by PS-PVD and further improvement of the coating was obtained by Al_2O_3-modification process, which covered the coating surface with a layer of dense α-Al_2O_3. The corrosion performance of the coatings under thermal exposure of NaCl and combustion gas-salt spray conditions was evaluated. The results show that NaCl has a strong attack on the thermal barrier coating, the as-sprayed coating has a catastrophic oxidation after corrosion, and the corrosion resistance of the Al_2O_3-modified coating has been significantly improved, effectively reducing the oxidation of metal layer.

NaCl mainly acts on the metal layer through the electrochemical corrosion mechanism. The main corrosion behavior is that Cl^- reacts with Al^{3+} at the TGO interface instead of O^{2-} to form the corrosion intermediate product AlO_2^-, and finally decomposes into Al_2O_3 to accelerate the thickening of TGO. In the combustion gas-hot corrosion test, the 7YSZ coating has obvious sintering phenomenon, but the sintering degree of the Al_2O_3-modified coating is lower than that of the as-sprayed coating due to less molten salt infiltration.

The feather-like columnar structure PS-PVD 7YSZ thermal barrier coatings faces greater hot corrosion challenges in the marine environment due to its unique structure. In this work, it may help to improve the service performance of the coating in the marine environment.

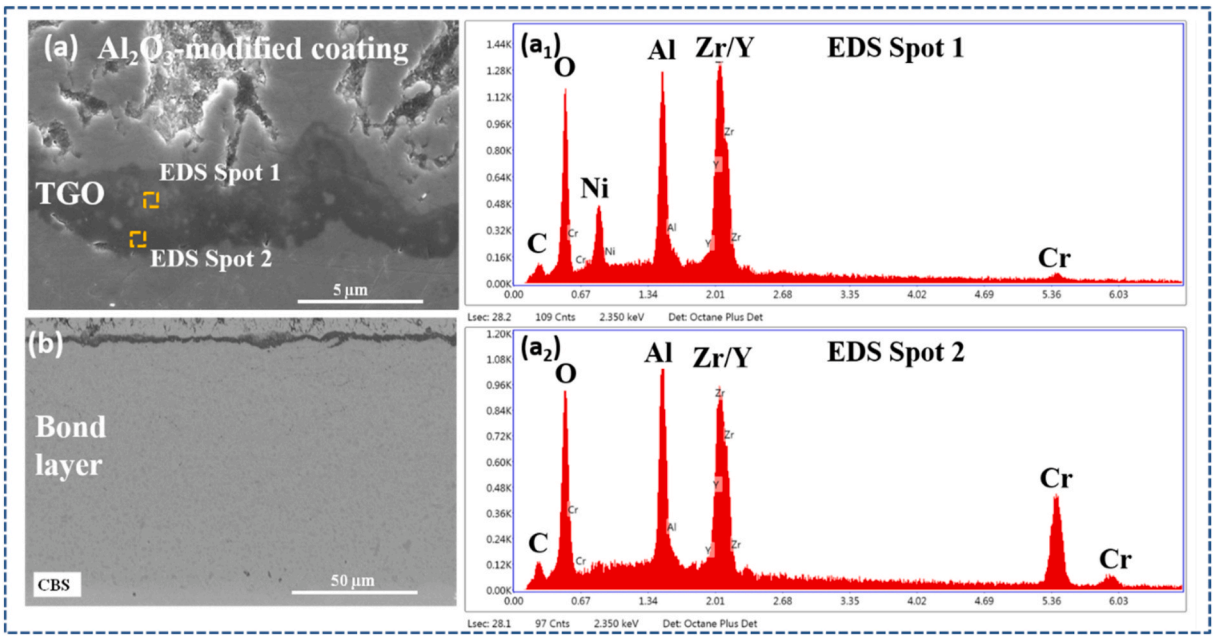

Fig. 15. Al_2O_3-modified coating after NaCl thermal exposure, (a) TGO morphology, (a1) and (a2) TGO element analysis. (b) Backscattered electron imaging of metal bonding layer.

Data availability statement

The data that support the findings of this study are openly available in Web of Science.

Declaration of interest

No conflict of interest exits in the submission of this manuscript, and manuscript is approved by all authors for publication. I would like to declare under my ethical responsibility that the submitted paper is original and has not been or is not being submitted to the peer review process to any other journal research.

Declaration of competing interest

The authors declare that they have no known competing financial interests or personal relationships that could have appeared to influence the work reported in this paper.

Acknowledgements

We would like to acknowledge the financial support from the National Natural Science Foundation of China (51801034, 51771059), Guangdong Province Outstanding Youth Foundation (2021B1515020038), Guangdong Special Support Program (2019BT02C629), Guangdong Academy of Sciences Program (2020GDASYL-20200104030). and Guangzhou Technical Research Program (201906010015). Acknowledgements the nano-indentation test supports from the Testing &Analysis Center, Institute of New Materials, Guangdong Academy of Sciences.

References

[1] D.R. Clarke, M. Oechsner, N.P. Padture, et al., Thermal-barrier coatings for more efficient gas-turbine engines, MRS Bull. 37 (2012) 891–898.
[2] V.P. Deodeshmukh, Evaluating the hot corrosion behavior of high-temperature alloys for gas turbine engine components, Metals Mater. Soc. 67 (2015) 2608–2614.
[3] E. Omar, H. Abu-Rub, F. Blaabjerg, Renewable energy resources: current status, future prospects and their enabling technology, Renew. Sustain. Energy Rev. 39 (2014) 748–764.
[4] N.P. Padture, M. Gell, E.H. Jordan, Thermal barrier coatings for gas-turbine engine applications, Science 296 (2002) 280–283.
[5] M.H. Chen, S.L. Zhu, F.H. Wang, High temperature oxidation of NiCrAlY, nanocrystalline and enamel-metal nano-composite coatings under thermal shock, Corrosion Sci. 100 (2015) 556–565.
[6] X.Q. Cao, R. Vassen, D. Stoever, Ceramic materials for thermal barrier coatings, J. Eur. Ceram. Soc. 24 (2004) 1–10.
[7] P. Fauchais, Understanding plasma spraying, J. Phys. Appl. Phys. 34 (2004) 86–108.
[8] C. Zhu, Y.G. Wang, L.N. An, et al., Microstructure and oxidation behavior of conventional and pseudo graded NiCrAlY/YSZ thermal barrier coatings produced by supersonic air plasma spraying process, Surf. Coating. Technol. 272 (2015) 121–128.
[9] N.J. Simms, P.J. Kilgallon, J.E. Oakey, Degradation of heat exchanger materials under biomass co-firing conditions, Mater. A. T. High. Temp. 24 (2007) 333–342.
[10] F. Pettit, Hot corrosion of metals and alloys, Oxid. Metals 76 (2011) 1–21.
[11] X.F. Zhang, Z.Q. Deng, H. Li, et al., Al_2O_3-modified PS-PVD 7YSZ thermal barrier coatings for advanced gas-turbine engines, NPJ Mater. Degrad. 4 (2020) 31.
[12] E. Reinhold, P. Botzler, C. Deus, EB-PVD process management for highly productive zirconia thermal barrier coating of turbine blades, Surf. Coating. Technol. 120 (1999) 77–83.
[13] X.Z. Chen, X.D. Liu, G.Y. Zhou, et al., 50-year evapotranspiration declining and potential causations in subtropical Guangdong province, southern China, Catena 128 (2015) 185–194.
[14] X.F. Zhang, K.S. Zhou, M. Liu, et al., Mechanisms governing the thermal shock and tensile fracture of PS-PVD 7YSZ TBC, Ceram. Int. 44 (2018) 3973–3980.
[15] G. Mauer, A. Hospach, R. VAßEN, Process development and coating characteristics of plasma spray-PVD, Surf. Coating. Technol. 220 (2013) 219–224.
[16] X.F. Zhang, K.S. Zhou, J.B. Song, et al., Deposition and CMAS corrosion mechanism of 7YSZ thermal barrier coatings prepared by plasma spray-physical vapor deposition, J. Inorg. Mater. 30 (2015) 287–293.
[17] G.J. Danek, State-of-the-art survey on hot corrosion in marine gas turbine engines, Nav. Eng. J. 77 (1965) 359–869.
[18] D.A. Shifler, Hot corrosion: a modification of reactants causing degradation, Mater. High Temp. 35 (2018) 225–235.
[19] Y. Niu, F. Gesmundo, F. Viani, et al., The corrosion of Ni3Al in a combustion gas with and without Na_2SO_4-NaCl deposits at 600-800°C, Oxid. Metals 42 (1994) 330–337.
[20] G.D. Asmundis, F. Gesmundo, C. Bottino, High-temperature corrosion of pure chromium in SO2 (700-1000°C), Oxid. Metals 14 (1980) 351–361.
[21] E. Kosieniak, K. Biesiada, J. Kaczorowski, et al., Corrosion failures in gas turbine hot components, J. Fail. Anal. Prev. 12 (2012) 330–337.
[22] G. Sreedhar, V.S. Raja, Hot corrosion of YSZ/Al_2O_3 dispersed NiCrAlY plasma-sprayed coatings in Na_2SO_4-10 wt.% NaCl melt, Corrosion Sci. 52 (2010) 2592–2602.
[23] I. Gurrappa, Identification of hot corrosion resistant MCrAlY based bond coatings for gas turbine engine applications, Surf. Coating. Technol. 139 (2001) 272–283.
[24] R.L. Jones, S.T. Gadomski, The hot corrosion of CoCrAlY turbine blade coatings by Na_2SO_4 and vaporous NaCl, J. Electrochem. Soc. (1977) 124.

[25] A. Xi, A. Zn, Z.B. Lei, et al., Influence of Al_2O_3 overlay on corrosion resistance of plasma sprayed yttria-stabilized zirconia coating in NaCl-KCl molten salt, Surf. Coating. Technol. 361 (2019) 432–437.
[26] A.H. Pakseresht, A. Kimiay, M. Hizacleh, et al., Microstructural study and hot corrosion behavior of bimodal thermal barrier coatings under laser heat treatment, Ceram. Int. 46 (2020).
[27] L. Guo, H. Xin, X.M. Zhang, et al., Effects of laser surface modification on phase stability and microstructures of thermal barrier coatings in V_2O_5 molten salt, Surf. Technol. 49 (2020) 41–48.
[28] R. Ghasemi, R. Shoja-Razavi, R. Mozafarinia, Laser glazing of plasma-sprayed nanostructured yttria stabilized zirconia thermal barrier coatings, Ceram. Int. 39 (2013) 9483–9490.
[29] P. Yi, J. Mostaghimi, L. Pershin, et al., Effects of laser surface remelting on the molten salt corrosion resistance of yttria-stabilized zirconia coating, Ceram. Int. 44 (2018), 226455-22655.
[30] C.D. O'Dowd, G.d. Leeuw, Marine aerosol production: a review of the current knowledge, Phil. Trans. Math. Phys. Eng. Sci. 365 (2007) 1753–1774.
[31] S. Ariharan, Ambreen Nisar, N. Balaji, et al., Carbon nanotubes stabilize high temperature phase and toughen Al_2O_3-based thermal barrier coatings, Compos. B Eng. 124 (2017) 76–87.
[32] O. Yasin, M.D. Kadir, C.K. Abdullah, Hot corrosion behavior of YSZ, $Gd_2Zr_2O_7$ and YSZ/$Gd_2Zr_2O_7$ thermal barrier coatings exposed to molten sulfate and vanadate salt, Appl. Surf. Sci. 438 (2018) 96–113.
[33] J.F. Fan, X.F. Zhang, K.S. Zhou, et al., Influence of Al-modification on CMAS corrosion resistance of PS-PVD 7YSZ thermal barrier coatings, J. Inorg. Mater. 34 (2019) 938–946.
[34] B.Z. Wang, D.X. Li, Z.H. Yang, et al., Microstructural evolution and mechanical properties of in situ nano Ta_4HfC_5 reinforced SiBCN composite ceramics, J. Adv. Ceram. 9 (2020) 739–748.
[35] M.H. Li, X.F. Sun, W.Y. Hu, et al., Hot corrosion of a single crystal Ni-base superalloy by Na-salts at 900°C, Oxid. Metals 65 (2006) 137–150.
[36] Y.S. Zhang, Fluxing mechanism of hot corrosion and its limitation, J. Chin. Soc. Corrosion Protect 12 (1992) 1–10.
[37] G. Sreedhar, V.S. Raja, Hot corrosion of YSZ/Al_2O_3 dispersed NiCrAlY plasma-sprayed coatings in Na_2SO_4-10 wt.% NaCl melt, Corrosion Sci. 52 (2010) 2592–2602.
[38] F. Pettit, Hot corrosion of metals and alloys, Oxid. Met. 76 (2011) 1–21.
[39] J. Stringer, High temperature corrosion problems in the electric power industry and their solution, High Temp. Corros. 6 (1986) 389.